Modeling of Nonlaminated Electromagnetic Suspension Systems

Lei Zhu and Carl R. Knospe, *Senior Member, IEEE*

***Abstract*—Eddy currents induced within nonlaminated electromagnetic actuators by time-varying magnetic fields have a strong effect on the dynamics and control of electromagnetic suspension systems. This paper examines the modeling of these suspension systems and resolves two important problems: 1) the effect of time-varying flotor position on electromagnetic force production and 2) the proper manner in which to model voltage-mode operation of the suspension. The models developed are explicit functions of actuator material and geometric properties. The investigation focuses on axisymmetric cylindrical electromagnetic actuators. Similar results are provided for nonlaminated actuators with C-core stators. Experimental results are presented that demonstrate the accuracy of the modeling approach.**

***Index Terms*—Active magnetic bearings, electromagnetic actuators, electromagnetic suspension, fractional-order systems.**

I. Introduction

NONCONTACT electromagnetic suspension systems have been studied for a variety of industrial and scientific applications, including rotating machinery (i.e., active magnetic bearings) [1], [2], metal conveyance [3], metal coating processes [4], photolithography [5], and tool servo systems [6]. Typically, the electromagnet's stator and the flotor (the levitated part) are composed of laminations so as to reduce eddy currents within the ferromagnetic material. As Faraday's law dictates, eddy currents will be induced in any conductor in response to a changing magnetic field. These eddy currents, in turn, generate a magnetic field that opposes the change in externally applied field. For electromagnetic suspension systems, the effect of eddy currents is a reduction in the time-varying component of the actuator force as well as a phase lag between actuator coil current and the force produced. The use of laminated construction, however, causes these effects to be negligible within the typical bandwidth of electromagnetic suspension systems (2–5 kHz). In some applications, however, laminated construction is contradictory to the magnetic suspension's purpose (e.g., in sheet metal conveyance) or is precluded due to cost or strength concerns. An important example of the later is thrust magnetic bearings in rotating machinery, which rarely contain laminations. In such applications, eddy currents will have profound effects upon the behavior of the electromagnetic suspension system and must be considered in system modeling and controller design.

The dynamics of nonlaminated magnetic actuators was first studied by Zmood *et al.* [7], who examined a nonlaminated C-core electromagnet having a large ratio of pole width to height. Zmood *et al.* employed a one-term expansion of the model of Stoll [8] and derived a first-order analytic model. Feeley [9] also examined C-core actuators but used a 2-D eddy current formulation (also from Stoll). After an *ad hoc* approximation, a fractional-order transfer function model between perturbation current and force was obtained. In both papers, the authors assumed that the distribution of flux density in a cross section of air gap was identical to that in a cross section of the pole iron. As was shown in [10], this is not accurate in harmonic analysis due to the effects of eddy currents. Kucera and Ahrens [11] investigated the dynamics of a nonlaminated cylindrical magnetic actuator. In developing their analytic model, it was assumed that the air gap flux density was uniformly distributed and was independent of the frequency of the harmonic field. Furthermore, a parameter in this model must be determined from experimentation, as it does not correspond to any geometric or material property of the actuator.

In [10] and [12], the authors presented analytic results that describe the current–force relationship for cylindrical and C-core stators, respectively. The modeling approach used made no assumption regarding the distribution of field within the air gap and captured the effects of changing flux distribution with harmonic frequency. The analytic models obtained were explicit functions of actuator material and geometric properties. The analytical models obtained, however, were quite involved, consisting of transfer functions containing Bessel, hyperbolic tangent, hyperbolic cosine, or other infinite sums in fractional powers of the Laplace transform variable s. In [10] and [12], the authors reduced these models to simple fractional-order transfer functions in which all coefficients were explicit function of actuator material and geometric properties.

Two fundamental modeling issues of nonlaminated electromagnetic actuation have so far not been examined in any of the previous investigations: 1) the manner in which dynamic variations in flotor position (i.e., gap variations) affects the force applied to the flotor and 2) the relationship between voltage applied to the electromagnet's coil and the force induced upon the flotor. Resolution of these issues is essential to developing a complete model of nonlaminated electromagnetic suspension systems. In this paper, a solution settling these outstanding issues is provided. Furthermore, this solution is written explicitly in terms of actuator material and geometric properties. As a

Manuscript received May 2, 2008; revised July 28, 2008. First published April 21, 2009; current version published November 18, 2009. Recommended by Technical Editor W.-J. Kim. This work was supported by the National Science Foundation under Grant DMII-9988877.

L. Zhu is with Calnetix, Inc., Cerritos, CA 90703 USA (e-mail: lzhu@calnetix.com).

C. R. Knospe is with the Department of Mechanical and Aerospace Engineering, University of Virginia, Charlottesville, VA 22904 USA (e-mail: knospe@virginia.edu).

Color versions of one or more of the figures in this paper are available online at http://ieeexplore.ieee.org.

Digital Object Identifier 10.1109/TMECH.2009.2016656

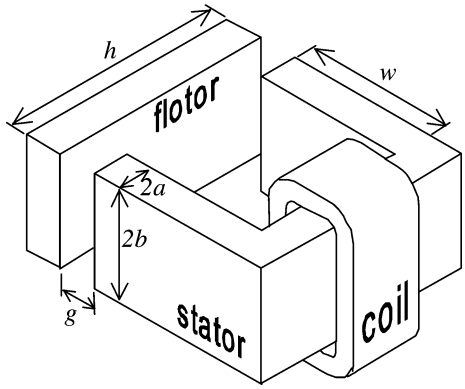

Fig. 1. Electromagnetic stator (C-core) acting upon a flotor with air gap g.

result, the model allows the characterization of configurations for which the effect of eddy currents is substantial. Largely, we will focus our investigation on nonlaminated cylindrical actuators. Similar results may be straightforwardly derived for other actuator configurations. Experimental results are provided that confirm the theory presented.

II. Preliminaries

A. Laminated Electromagnetic Suspensions

Our examination begins by reviewing electromagnetic suspension systems with laminated ferromagnetic components and amplifiers operating in current mode. Consider a single laminated electromagnetic stator acting upon a laminated flotor, as depicted in Fig. 1. The relationship between coil current *i* and force applied *f* is (approximately) given by

$$f = \beta \frac{N^2 i^2}{g^2} \tag{1}$$

where *N* and *g* are the number of coil turns and the gap between flotor and stator, respectively, and β is a constant dependent upon actuator geometry and size. As the actuator can only pull upon the flotor, to achieve a stable suspension, an opposing force must be provided by some other means, for example, by another actuator or by gravity acting upon the flotor. Thus, in equilibrium at a desired flotor position (gap length g_0), a bias force f_0 and current i_0 must be employed, where these quantities are related by

$$f_0 = \beta \frac{N^2 i_0^2}{g_0^2}.$$

Linearization of (1) about this equilibrium yields

$$f_p = K_i i_p + K_g g_p \tag{2}$$

where f_p, i_p, and g_p are variations in force, current, and gap from operating point values (f_0, i_0, g_0)

$$f_p = f - f_0 \qquad i_p = i - i_0 \qquad g_p = g - g_0 \tag{3}$$

and the coefficients are given by

$$K_i = \left.\frac{\partial f}{\partial i}\right|_{\substack{g=g_0 \\ i=i_0}} > 0 \qquad K_g = \left.\frac{\partial f}{\partial g}\right|_{\substack{g=g_0 \\ i=i_0}} < 0. \tag{4}$$

Variable i_p is commonly referred to as the perturbation current. We note that the actuator force *f* is directed opposite the positive direction for gap perturbation g_p. We will choose the positive direction for flotor displacement x to be the same as the positive direction for actuator force *f*. Thus, flotor displacement will be equal to the negative of gap perturbation, i.e., $x = -g_p$. (This choice of variables and axes is common in the literature.) The flotor displacement will be determined by the actuator force and the flotor compliance *H*(*s*) via the relationship

$$X(s) = H(s) F_p(s) \tag{5}$$

where $F_p(s)$ and *X*(*s*) are Laplace transforms of signals f_p and x. Define

$$K_x = \left.\frac{\partial f}{\partial x}\right|_{\substack{g=g_0 \\ i=i_0}} = -K_g.$$

As $x = -g_p$, (2) may be rewritten after Laplace transformation as

$$F_p(s) = K_i I_p(s) + K_x X(s) \tag{6}$$

where $I_p(s)$ is the Laplace transform of the perturbation current, $I_p(s) = \mathcal{L}\{i_p(t)\}$. Equations (5) and (6) form the conventionally used model of a laminated electromagnetic suspension system (no eddy currents) operated in current mode.

B. Approach to the Nonlaminated Problem

For actuators composed partly or entirely of solid (i.e., *nonlaminated*) ferromagnetic components, the model given in (6) is not accurate in practice due to the effect of eddy currents within the solid components. In [10], the authors developed an analytical model for nonlaminated cylindrical magnetic actuators that expressed the relationship between perturbation current and perturbation force when gap variation was negligible. We will recap the solution method and results here as a precursor to the next section.

The actuator geometry considered first is axisymmetric, as is the flux distribution inside the actuator. The actuator and its cross section are shown in Fig. 2 with all the dimensional notations used throughout this paper. A cylindrical coordinate system (r, φ, z) is employed. Hysteresis, magnetic saturation, and flux fringing are beyond the scope of this paper; only linear isotropic materials are considered. We assume that both the stator and flotor are not laminated, and that they have equal electrical conductivity, denoted by σ, and equal relative permeability, denoted by μ_r.

Our approach to analysis, like that in [10], considers the problem as several 1-D problems linked together via a magnetic circuit framework. The actuator geometry is divided into six elements, as illustrated in Fig. 3. This division is based on the direction of flux lines observed in finite-element analysis of the actuator; a detailed discussion may be found in [10]. Elements 1 and 3 consist of thin sections of the iron and the corresponding air gaps between the stator and flotor. Flux in these elements is radially directed in the transition regions of the iron and is parallel to the z-axis in the air gap. In elements 2 and 5, the flux is assumed to be parallel to the radial direction, while in

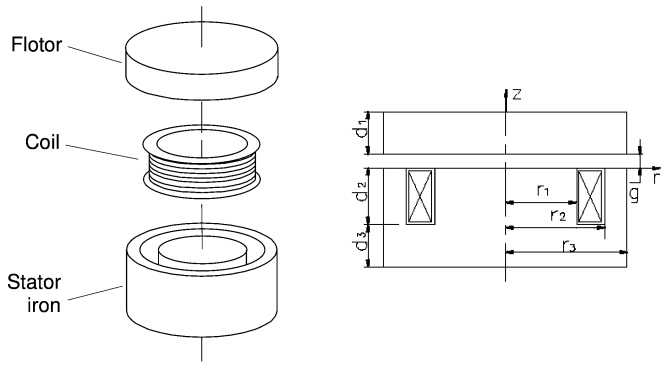

Fig. 2. Exploded view and cross section of a nonlaminated electromagnetic actuator.

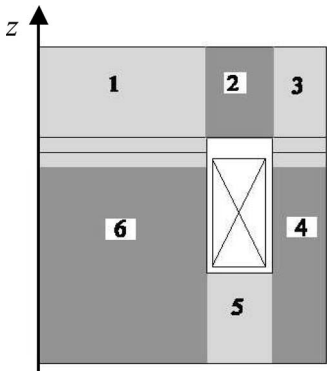

Fig. 3. Six elements used in analysis. The z-axis is the line of circular symmetry.

elements 4 and 6, it is parallel to the z-axis. In [10], the effective reluctance of each of these elements was derived from formulating and solving ordinary differential equations governing the field strength, determining the flux density and effective permeability, and integrating.

III. Current-Mode Model With Time-Varying Displacement

A. Model of Elements With Time-Varying Air Gaps

We now consider modeling elements 1 and 3 when the flotor position, and hence gap length, is time-varying. This is treated as a time-varying perturbation g_p added to the nominal gap g_0. In this case, the flux within the actuator may be considered to consist of two parts: a bias flux and a perturbation flux. The bias flux distribution will typically display nearly uniform flux density along both the stator and flotor surfaces and within the air gap (see [10] for details) while the distribution of the perturbation flux will be similar to that considered for the varying field in [10], spatially nonuniform with this distribution dependent on the frequency of variation. Assuming that the iron may be reasonably approximated as possessing a linear magnetization curve with relative permeability μ_r, superposition of the time-varying and constant flux densities may be employed in analysis.

We introduce a reluctance network, shown in Fig. 4, to model element 1. This consists of nodes in the flotor and stator with

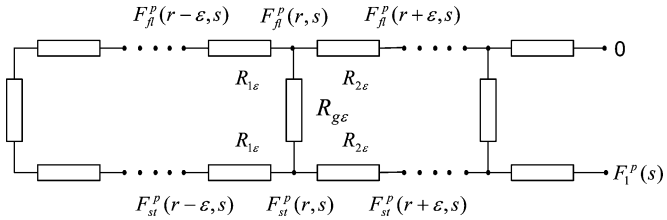

Fig. 4. Reluctance network for element 1.

flux paths directed radially in the iron and parallel to the z-axis in the air gap. The effective reluctances of the paths in the iron from a node at radius r to nodes at radius $r-\varepsilon$ and $r+\varepsilon$ are, respectively, given by

$$R_{1\varepsilon} = \frac{\varepsilon\alpha}{2\pi\left(r-(\varepsilon/2)\right)\mu_r\mu_0} \qquad R_{2\varepsilon} = \frac{\varepsilon\alpha}{2\pi\left(r+(\varepsilon/2)\right)\mu_r\mu_0} \tag{7}$$

where $\alpha = \sqrt{s\sigma\mu_r\mu_0}$. These reluctances account for the frequency-dependent nature of axial thickness of the iron paths [10].

We now turn our attention to modeling the air gap paths in the reluctance network. Consider a small annular section of inner pole's air gap at radius r and with radial thickness ε. The time-varying reluctance of this section may be expressed as

$$R_{g\varepsilon} = \frac{g_0 + g_p(t)}{2\pi r\varepsilon\mu_0} \tag{8a}$$

where μ_0 is the permeability of free space. Note that the time dependence of the perturbation term is explicitly indicated (t). Define the nominal reluctance of this gap section as

$$R_{g\varepsilon}^n = \frac{g_0}{2\pi r\varepsilon\mu_0}. \tag{8b}$$

Assuming that $g_p(t)$ is small in comparison to the nominal value g_0, the flux passing through reluctance $R_{g\varepsilon}$ at any time t, is

$$\begin{aligned}\phi_\varepsilon(r,t) &= \frac{f_{st}(r,t) - f_{fl}(r,t)}{R_{g\varepsilon}} \\ &\approx \frac{f_{st}(r,t) - f_{fl}(r,t)}{R_{g\varepsilon}^n}\left(1 - \frac{g_p(t)}{g_0}\right)\end{aligned} \tag{9}$$

where $f_{fl}(r,t)$ and $f_{st}(r,t)$ are the magnetomotive forces on the surfaces of the flotor and stator, respectively. These quantities may be considered to consist of bias and perturbation terms; hence,

$$f_{fl}(r,t) = f_{fl}^b(r) + f_{fl}^p(r,t) \tag{10a}$$

$$f_{st}(r,t) = f_{st}^b(r) + f_{st}^p(r,t). \tag{10b}$$

Substituting (8) into (9) yields

$$\begin{aligned}\phi_\varepsilon(r,t) = &\frac{1}{R_{g\varepsilon}^n}\left[f_{st}^b(r) - f_{fl}^b(r)\right] \\ &- \frac{1}{R_{g\varepsilon}^n}\left[f_{st}^b(r) - f_{fl}^b(r)\right]\frac{g_p(t)}{g_0}\end{aligned}$$

$$+\frac{1}{R^n_{g\varepsilon}}\left[f^p_{st}(r,t)-f^p_{fl}(r,t)\right]$$
$$-\frac{1}{R^n_{g\varepsilon}}\left[f^p_{st}(r,t)-f^p_{fl}(r,t)\right]\frac{g_p(t)}{g_0}. \quad (11)$$

We will assume that magnetomotive perturbation terms are small in comparison to the nominal values and so neglect the higher order terms in (11). The flux may be separated into time-invariant (bias, ϕ^b_ε) and time-varying (perturbation, $\phi^p_\varepsilon(r,t)$) components

$$\phi_\varepsilon(r,t)=\phi^b_\varepsilon(r)+\phi^p_\varepsilon(r,t) \quad (12a)$$
$$\phi^b_\varepsilon(r)=\frac{1}{R^n_{g\varepsilon}}\left[f^b_{st}(r)-f^b_{fl}(r)\right] \quad (12b)$$
$$\phi^p_\varepsilon(r,t)=-\frac{1}{R^n_{g\varepsilon}}\left[f^b_{st}(r)-f^b_{fl}(r)\right]\frac{g_p(t)}{g_n}$$
$$+\frac{1}{R^n_{g\varepsilon}}\left[f^p_{st}(r,t)-f^p_{fl}(r,t)\right]. \quad (12c)$$

To simplify analysis, we assume a uniform bias flux distribution in the gaps. (While generally quite accurate, this assumption is not necessary for the overall approach.) In this case, the bias magnetomotive forces are related by

$$f^b_{st}(r)-f^b_{fl}(r)=\frac{Ni_0R^0_1}{R^0} \quad (13)$$

where R^0_1 is the static reluctance of element 1 (with fixed air gap g_0), R^0 is the static reluctance of the entire actuator flux path

$$R^0=\sum_{k=1}^{6}R^0_k$$

and R^0_k is the static reluctance of element *k*. Combining (12) and (13) yields

$$\phi^b_\varepsilon=\frac{1}{R^n_{g\varepsilon}}\frac{Ni_0R^0_1}{R^0} \quad (14a)$$
$$\phi^p_\varepsilon(r,t)=-\frac{1}{R^n_{g\varepsilon}}\frac{Ni_0R^0_1}{R^0}\frac{g_p(t)}{g_0}$$
$$+\frac{1}{R^n_{g\varepsilon}}\left[f^p_{st}(r,t)-f^p_{fl}(r,t)\right]. \quad (14b)$$

After Laplace transformation ($\mathcal{L}$), (14b) becomes

$$\phi^p_\varepsilon(r,s)=\mathcal{L}\left(\phi^p_\varepsilon(r,t)\right)$$
$$=-\frac{1}{R^n_{g\varepsilon}}\frac{Ni_0R^0_1}{R^0}\frac{g_p(s)}{g_0}$$
$$+\frac{1}{R^n_{g\varepsilon}}\left[F^p_{st}(r,s)-F^p_{fl}(r,s)\right]. \quad (14c)$$

Conservation of flux for the node at radius *r* provides the equation

$$\phi^p_\varepsilon(r,s)+\frac{F^p_{st}(r,s)-F^p_{st}(r-\varepsilon,s)}{R_{1\varepsilon}}=\frac{F^p_{st}(r+\varepsilon,s)-F^p_{st}(r,s)}{R_{2\varepsilon}}. \quad (15)$$

Due to the symmetry of the reluctance network, we have

$$F^p_{fl}(r,s)=F^p_1(s)-F^p_{st}(r,s). \quad (16)$$

Substituting (14c) and (16) into (15) yields

$$\frac{F^p_{st}(r+\varepsilon,s)-F^p_{st}(r,s)}{R_{2\varepsilon}}$$
$$=\frac{F^p_{st}(r,s)-F^p_{st}(r-\varepsilon,s)}{R_{1\varepsilon}}+\frac{2F^p_{st}(r,s)}{R^n_{g\varepsilon}}$$
$$-\frac{F^p_1(s)}{R^n_{g\varepsilon}}-\frac{1}{R^n_{g\varepsilon}}\frac{Ni_0R^0_1}{R^0}\frac{g_p(s)}{g_0}. \quad (17)$$

Taking the limit of (17) as $\varepsilon\to 0$ yields the ordinary differential equation

$$\frac{d^2F^p_{st}(r,s)}{dr^2}+\frac{1}{r}\frac{dF^p_{st}(r,s)}{dr}-\alpha_1^2F^p_{st}(r,s)$$
$$=-\frac{\alpha_1^2}{2}F^p_1(s)-\frac{\alpha_1^2}{2}\frac{Ni_0R^0_1}{R^0}\frac{g_p(s)}{g_0} \quad (18)$$

where $\alpha_1^2=2\alpha/\mu_r g_0$. From the analysis in [10], the solution to (18) is given by

$$F^p_{st}(r,s)=\frac{F^p(s)}{2}+\frac{1}{2}\frac{Ni_0R^0_1}{R^0}\frac{g_p(s)}{g_0}$$
$$+\left(\frac{F^p_1(s)}{2}-\frac{1}{2}\frac{Ni_0R^0_1}{R^0}\frac{g_p(s)}{g_0}\right)\frac{I_0(\alpha_1 r)}{I_0(\alpha_1 r_1)} \quad (19a)$$

where $I_0(\cdot)$ is the zero-order modified Bessel function of the first kind. From (16) and (19a), we obtain

$$F^p_{fl}(r,s)=\frac{F^p(s)}{2}-\frac{1}{2}\frac{Ni_0R^0_1}{R^0}\frac{g_p(s)}{g_0}$$
$$-\left(\frac{F^p_1(s)}{2}-\frac{1}{2}\frac{Ni_0R^0_1}{R^0}\frac{g_p(s)}{g_0}\right)\frac{I_0(\alpha_1 r)}{I_0(\alpha_1 r_1)}. \quad (19b)$$

Substituting (19) into (14c) yields the perturbation flux through the air gap at radius *r*

$$\phi^p_\varepsilon(r,s)=\frac{1}{R^n_{g\varepsilon}}\left(F^p_1(s)-\frac{Ni_0R^0_1}{R^0}\frac{g_p(s)}{g_0}\right)\frac{I_0(\alpha_1 r)}{I_0(\alpha_1 r_1)}. \quad (20)$$

The perturbation flux through the entire inner pole air gap may then be found via integration

$$\phi_p(s)=\int_0^{r_1}\phi^p_\varepsilon(r,s)dr$$
$$=\frac{2\pi\mu_0 r_1 I_1(\alpha_1 r_1)}{g_0\alpha_1 I_0(\alpha_1 r_1)}\left(F^p_1(s)-\frac{Ni_0R^0_1}{R^0}\frac{g_p(s)}{g_0}\right)$$
$$=\frac{1}{R_1}\left(F^p_1(s)-\frac{Ni_0R^0_1}{R^0}\frac{g_p(s)}{g_0}\right) \quad (21)$$

where R_1 is the effective reluctance of element 1 with nominal air gap g_0

$$R_1=\frac{g_0\alpha_1 I_0(\alpha_1 r_1)}{2\pi\mu_0 r_1 I_1(\alpha_1 r_1)}$$

and $I_1(\cdot)$ is the first-order modified Bessel function of the first kind.

Using this approach for element 3, a similar relationship can be derived

$$\phi_p(s) = \frac{1}{R_3}\left(F_3^p(s) - \frac{Ni_0R_3^0}{R^0}\frac{g_p(s)}{g_0}\right) \tag{22}$$

where R_3 is the effective reluctance of element 3 with nominal air gap g_0 and $F_3^p(s)$ is the perturbation magnetomotive force across this element. The effective reluctance is given by

$$R_3 = \frac{g_0}{2\pi r_2\mu_0}\frac{\alpha_1\left[I_0(\alpha_1 r_2)K_1(\alpha_1 r_3) + K_0(\alpha_1 r_2)I_1(\alpha_1 r_3)\right]}{K_1(\alpha_1 r_2)I_1(\alpha_1 r_3) - I_1(\alpha_1 r_2)K_1(\alpha_1 r_3)}$$

where $K_0(\cdot)$ and $K_1(\cdot)$ are the zero-order and first-order modified Bessel functions of the second kind.

Both (21) and (22) may be rewritten in the form

$$F_k^p(s) = R_k\phi_p(s) + \frac{Ni_0R_k^0}{R^0}\frac{g_p(s)}{g_0}, \qquad k = 1, 3. \tag{23}$$

B. Actuator Electromagnetic Model

We now turn our attention to those elements that do not include air gaps (elements 2, 4, 5, and 6). The results found in [10] need no modification for the purposes of our current investigation. For each of these elements, the perturbation magnetomotive force across the element $F_k^p(s)$ is related to the perturbation flux through it by an equation of the form

$$F_k^p(s) = R_k\phi_p(s), \qquad k = 2, 4, 5, 6 \tag{24}$$

where the reluctances R_k are summarized in Table I. The magnetomotive force across each element consists of a bias term and a perturbation term, expressed in the time domain as

$$f_k(t) = f_k^b + f_k^p(t) \tag{25}$$

where the bias terms are constant. Applying Ampere's law to the magnetic circuit composed of the six elements in series yields

$$\sum_{k=1}^{6} f_k(t) = Ni(t). \tag{26a}$$

For the static bias field, this may be reduced to

$$\sum_{k=1}^{6} f_k^b = Ni_0 \tag{26b}$$

and, therefore, the perturbation terms are governed by

$$\sum_{i=1}^{6} f_i^p(t) = Ni_p(t)$$

or, after Laplace transformation,

$$\sum_{i=1}^{6} F_i^p(s) = NI_p(s). \tag{27}$$

Substituting (23) and (24) into (27) yields

$$\phi_p(s)\sum_{k=1}^{6} R_k + \frac{Ni_0R_1^0}{R^0}\frac{g_p(s)}{g_0} + \frac{Ni_0R_3^0}{R^0}\frac{g_p(s)}{g_0} = NI_p(s). \tag{28}$$

Noting that $R_1^0 = g_0/\mu_0A_1$ and $R_3^0 = g_0/\mu_0A_3$, where A_1 and A_3 are the cross-sectional areas of the inner and outer poles, respectively, the perturbation flux may be found

$$\phi_p(s) = \frac{N}{\sum_{k=1}^{6} R_k}I_p(s) - \frac{1}{\mu_0}\left(\frac{1}{A_1} + \frac{1}{A_3}\right)\frac{Ni_0}{R^0}\frac{1}{\sum_{k=1}^{6} R_k}g_p(s). \tag{29}$$

With the air-gap flux assumed to be parallel to the z-axis, the mechanical force applied to the flotor may be determined using Maxwell stress tensor

$$f(t) = \frac{1}{2\mu_0}\oint_S B^2(r,t)dA = \frac{1}{2\mu_0}\oint_S \left[B_0^2(r) + 2B_0(r)B_p(r,t) + B_p^2(r,t)\right]2\pi r\,dr \tag{30}$$

where B, B_0, and B_p are the total, bias, and perturbation flux densities in the air gap, respectively, and S is a surface between the flotor and stator. Assuming that the perturbation flux density is small in comparison to the bias flux density, the time-varying component of mechanical force may be found

$$\begin{aligned} f_p(t) &= \frac{1}{\mu_0}\oint_S B_0(r)B_p(r,t)\,2\pi r\,dr \\ &= \frac{1}{\mu_0}\oint_{S_1}\left(\frac{\phi_0}{A_1}\right)B_p(r,t)\,2\pi r\,dr \\ &\quad + \frac{1}{\mu_0}\oint_{S_3}\left(\frac{\phi_0}{A_3}\right)B_p(r,t)\,2\pi r\,dr \end{aligned} \tag{31}$$

where S_1 and S_3 are projections of the inner pole face and outer pole face on surface S. We note that

$$\oint_{S_1} B_p(r,t)\,2\pi r\,dr = \oint_{S_3} B_p(r,t)\,2\pi r\,dr = \phi_p(t). \tag{32}$$

Therefore, the total mechanical force is given by

$$f_p(t) = \frac{1}{\mu_0}\left(\frac{1}{A_1} + \frac{1}{A_3}\right)\phi_0\phi_p(t). \tag{33}$$

The bias flux ϕ_0 may be found via

$$\phi_0 = \frac{Ni_0}{R^0} \tag{34}$$

where R^0 is the total static reluctance of the flux circuit. Substitution of (34) into (33) and Laplace transformation yields the perturbation force in terms of the perturbation flux

$$F_p(s) = K_\phi\phi_p(s) \tag{35}$$

where

$$K_\phi = \frac{1}{\mu_0}\left(\frac{1}{A_1} + \frac{1}{A_3}\right)\frac{Ni_0}{R^0}. \tag{36}$$

We note that K_ϕ also appears in (29), which may be rewritten as

$$\phi_p(s) = \frac{N}{\sum_{k=1}^{6} R_k}I_p(s) - K_\phi\frac{1}{\sum_{k=1}^{6} R_k}g_p(s). \tag{37}$$

TABLE I
EFFECTIVE RELUCTANCES OF THE ELEMENTS AND THEIR APPROXIMATIONS

i	Effective Reluctance $R_i(s)$	Approximation	
		R_i^0	c_i
1	$\frac{g\alpha_1 I_0(\alpha_1 r_1)}{2\pi\mu_0 r_1 I_1(\alpha_1 r_1)}$ *	$\frac{g_0}{\pi r_1^2 \mu_0}$	$\frac{1}{4\pi}\sqrt{\frac{\sigma}{\mu_r\mu_0}}$
2	$\frac{\ln(r_2/r_1)}{2\pi\mu_r\mu_0}\frac{\alpha}{\tanh(\alpha d_1)}$ **	$\frac{\ln(r_2/r_1)}{2\pi d_1\mu_r\mu_0}$	$\frac{\ln(r_2/r_1)}{2\pi}\sqrt{\frac{\sigma}{\mu_r\mu_0}}$
3	$\frac{g}{2\pi\mu_0 r_2}\cdot\frac{\alpha_1[I_0(\alpha_1 r_2)K_1(\alpha_1 r_3)+K_0(\alpha_1 r_2)I_1(\alpha_1 r_3)]}{K_1(\alpha_1 r_2)I_1(\alpha_1 r_3)-I_1(\alpha_1 r_2)K_1(\alpha_1 r_3)}$	$\frac{g_0}{\pi\mu_0(r_3^2-r_2^2)}$	$\frac{(2r_3^4\ln\frac{r_3}{r_2}-\frac{3}{2}r_3^4+2r_2^2r_3^2-\frac{1}{2}r_2^4)}{2\pi(r_3^2-r_2^2)^2}\times\sqrt{\frac{\sigma}{\mu_r\mu_0}}$
4	$\frac{d_2}{2\pi\mu_r\mu_0 r_2}\cdot\frac{\alpha[I_0(\alpha r_2)K_1(\alpha r_3)+K_0(\alpha r_2)I_1(\alpha r_3)]}{K_1(\alpha r_2)I_1(\alpha r_3)-I_1(\alpha r_2)K_1(\alpha r_3)}$	$\frac{d_2}{\pi\mu_r\mu_0(r_3^2-r_2^2)}$	$\frac{d_2}{2\pi r_2}\sqrt{\frac{\sigma}{\mu_r\mu_0}}$
5	$\frac{\ln(r_2/r_1)}{2\pi\mu_r\mu_0}\frac{\alpha}{\tanh(\alpha d_3)}$	$\frac{\ln(r_2/r_1)}{2\pi d_3\mu_r\mu_0}$	$\frac{\ln(r_2/r_1)}{2\pi}\sqrt{\frac{\sigma}{\mu_r\mu_0}}$
6	$\frac{d_2}{2\pi r_1\mu_r\mu_0}\frac{\alpha I_0(\alpha r_1)}{I_1(\alpha r_1)}$	$\frac{d_2}{\pi r_1^2\mu_r\mu_0}$	$\frac{d_2}{2\pi r_1}\sqrt{\frac{\sigma}{\mu_r\mu_0}}$

*: $\alpha_1 = \sqrt{2\alpha/\mu_r g}$. **: $\alpha = \sqrt{s\sigma\mu_r\mu_0}$.

Combining (35) and (37) yields the model

$$F_p(s) = K_\phi \frac{N}{\sum_{k=1}^{6} R_k} I_p(s) - K_\phi^2 \frac{1}{\sum_{k=1}^{6} R_k} g_p(s). \quad (38a)$$

Since $x = -g_p$, this equation may be alternatively expressed as

$$F_p(s) = K_\phi \frac{N}{\sum_{k=1}^{6} R_k} I_p(s) + K_\phi^2 \frac{1}{\sum_{k=1}^{6} R_k} X(s). \quad (38b)$$

C. Simplified Model

The analytical expressions for the reluctances of the six elements (Table I) contain complex functions (i.e., hyperbolic tangent and modified Bessel functions) that make the result of (38) difficult to employ in design or tradeoff studies. In [10], the authors presented a detailed study of various approximations for R_k. This study demonstrated that each reluctance could be approximated with high accuracy using the form

$$\tilde{R}_k = R_k^0 + c_k\sqrt{s}$$

where R_k^0 is the static reluctance of element k and c_k is an eddy current coefficient for element k. The analytic expressions for these parameters are also listed in Table I. Note that both R_k^0 and c_k are explicit functions of actuator material and geometric properties.

Using these approximations, the sum of the element reluctances may be approximated as

$$\sum_{k=1}^{6} R_k \approx R^0 + c\sqrt{s} \quad (39a)$$

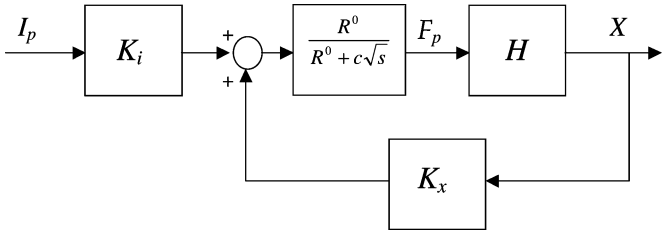

Fig. 5. Block diagram of a nonlaminated electromagnetic suspension system operated in current mode.

with

$$R^0 = \sum_{k=1}^{6} R_k^0 \quad c = \sum_{k=1}^{6} c_k. \tag{39b}$$

Employing (39a) and (39b), the perturbation force may be determined as

$$F_p(s) = K_\phi \frac{N}{R^0 + c\sqrt{s}} I_p(s) - K_\phi^2 \frac{1}{R^0 + c\sqrt{s}} g_p(s) \tag{40}$$

or

$$F_p(s) = K_\phi \frac{N}{R^0 + c\sqrt{s}} I_p(s) + K_\phi^2 \frac{1}{R^0 + c\sqrt{s}} X(s). \tag{41}$$

We note that K_ϕ is related to the parameters K_i and K_x introduced in Section II for the case of laminated actuator (i.e., no eddy currents)

$$K_i = \frac{K_\phi N}{R^0} \quad K_x = \frac{K_\phi^2}{R^0}. \tag{42a}$$

Hence, (41) may be expressed as

$$F_p(s) = K_i \frac{R^0}{R^0 + c\sqrt{s}} I_p(s) + K_x \frac{R^0}{R^0 + c\sqrt{s}} X(s) \tag{42b}$$

which indicates that the effect of eddy currents is to introduce the transfer function $R^0/\left(R^0 + c\sqrt{s}\right)$ into the relationships between current/displacement and force. As coefficient c approaches zero (no eddy currents), the model of the laminated magnetic suspension system (6) is recovered.

A block diagram model of a nonlaminated actuator operated in current mode is illustrated in Fig. 5. If parameter c is set equal to zero in this model, the block diagram for the laminated system, formed from (5) and (6), will be recovered. The transfer function from perturbation current to flotor displacement is

$$\frac{X(s)}{I_p(s)} = \frac{K_i R^0 H(s)}{c\sqrt{s} + R^0 - K_x R^0 H(s)}. \tag{43}$$

This model is a *fractional-order system* as a fractional-order power of variable s appears in the transfer function. There has been considerable interest recently in the stability and control of such systems; the interested reader is referred to [13].

IV. Model of Nonlaminated C-Core Actuator

We now consider a C-core electromagnetic actuator with geometry shown in Fig. 1. Denote pole face area as A ($A = 4ab$) and iron path length as l ($l = 2w + 2h$).

A procedure similar to that employed for the cylindrical actuator may be followed in this case. Here, we present only the resulting simplified model, which is of the same form as (41), but with coefficients

$$K_\phi = \frac{1}{\mu_0}\left(\frac{2}{A}\right)\frac{Ni_0}{R^0} \tag{44a}$$

$$R^0 = \frac{1}{\mu_0 A}\left(2g_0 + \frac{l}{\mu_r}\right) \tag{44b}$$

$$c = \left[\frac{l}{4(a+b)} + \frac{b}{3a} - \frac{64b^2}{\pi^5 a^2}\tanh\left(\frac{\pi a}{2b}\right)\right]\sqrt{\frac{\sigma}{\mu_r \mu_0}}. \tag{44c}$$

V. Model for Voltage-Mode Operation

A. Model

Consider a nonlaminated actuator driven by a power amplifier operated in voltage mode. The voltage across the coil, v, is related to the coil current and total flux via

$$v(t) = \mathcal{R} i + N\frac{d\phi}{dt} \tag{45}$$

where $\mathcal{R}$ is the coil's resistance. The same relationship holds for the perturbations

$$v_p(t) = \mathcal{R} i_p(t) + N\frac{d\phi_p}{dt}(t) \tag{46}$$

where $v_p = v - v_0$. Taking the Laplace transform of (46) yields

$$V_p(s) = \mathcal{R} I_p(s) + sN\phi_p(s). \tag{47}$$

Equations (5), (29), (35), and (47) together form a model of a nonlaminated actuator operated in voltage mode. Two equivalent block diagram representations of this model are shown in Fig. 6.

B. Observations

From the block diagrams, two important observations can be made regarding the input–output behavior of a nonlaminated actuator operated in voltage mode. First, for any operating point (i.e., g_0, i_0), the effect of eddy currents on the frequency response of the transfer functions $F_p(s)/V_p(s)$ and $X(s)/V_p(s)$ occurs only in a middle band of frequencies. This observation can be seen easily from Fig. 6(b). The inner loop transfer function is

$$\frac{N}{N^2 s + c\mathcal{R}\sqrt{s} + R^0\mathcal{R}} \tag{48}$$

which is the sole element containing the eddy current coefficient c. The manner in which coefficient c enters into this transfer function indicates that the eddy current contribution to the dynamics will only be dominant in the frequency (ω) range

$$\frac{R^0}{c} << \sqrt{\omega} << \frac{c\mathcal{R}}{N^2}. \tag{49}$$

Our second observation considers the range of nominal gaps g_0 for which eddy currents will impact the frequency response

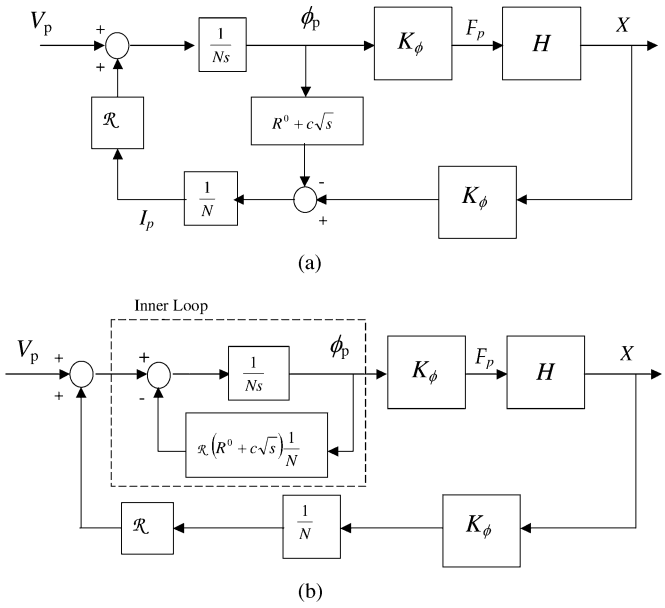

Fig. 6. Two equivalent block diagrams of a nonlaminated actuator operated in voltage mode.

$F_p(s)/V_p(s)$. We will show that such an effect will not occur when the gap is too large. Clearly, from (49), if the static reluctance of the flux path satisfies the condition

$$R^0 \geq \frac{c^2\mathcal{R}}{N^2}$$

then the effect of eddy currents on the frequency response will be negligible. Since the right-hand side of the inequality is independent of nominal gap g_0 and the left-hand side is affine in this quantity, this condition will be satisfied when the gap is sufficiently large. Hence, the effect of eddy currents on the frequency response will be minimal for actuators with large nominal gaps.

Interestingly, the effect of eddy currents may also be negligible in certain cases when the nominal gap g_0 is quite small. For this to occur, the actuator must have its iron path reluctance much smaller than that of the small air gap. Since $K_\phi \propto 1/R^0$, K_ϕ will be large in this case. Let us consider the implications of large values of K_ϕ on the frequency response of transfer function $F_p(s)/V_p(s)$. Simple algebra yields

$$\frac{F_p(s)}{V_p(s)} = \frac{NK_\phi}{N^2 s + \mathcal{R}c\sqrt{s} + \mathcal{R}R^0 - \mathcal{R}K_\phi^2 H(s)}. \quad (50)$$

If the flotor is not constrained by any flexure, $H(s)$ will be a type-2 system. In this case, the term $\mathcal{R}K_\phi^2 H(s)$ will dominate $\mathcal{R}c\sqrt{s}$ in the denominator over a low-frequency range. If K_ϕ is sufficiently large, this range may extend up to the frequencies where the term $N^2 s$ dominates $\mathcal{R}c\sqrt{s}$. In this case, the effect of eddy currents upon the frequency response will be minimal. Thus, in some actuators with small air gaps, the effect of eddy currents on the frequency response may be minor. Of course, the reader should note that if the air gap is too small, the assumptions regarding flux flow and distribution that were employed in developing the model (50) will be violated.

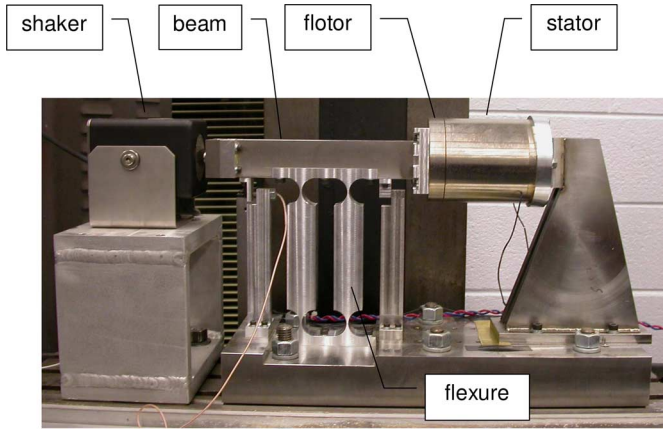

Fig. 7. Experiment for investigating nonlaminated electromagnetic actuation.

TABLE II
PROPERTIES OF NONLAMINATED ACTUATOR (SEE FIG. 3 FOR GEOMETRY)

Actuator Geometric Parameters	r_1	25 mm
	r_2	35 mm
	r_3	43 mm
	d_1	15 mm
	d_2	82 mm
	d_3	15 mm
Material		Nickel-iron, Carpenter Hyperm 49, dry hydrogen anneal
Coil turns, N		205
Coil resistance, $\mathcal{R}$		5.2 ohms

We now contrast these observations made for voltage-mode operation with the behavior for current-mode operation. The transfer function of interest in that case is

$$\frac{F_p(s)}{I_p(s)} = \frac{K_i R^0}{c\sqrt{s} + R^0 - K_x R^0 H(s)}. \quad (51)$$

Since $R^0 - K_x R^0 H(s)$ will dominate $c\sqrt{s}$ over low frequencies, the effect of eddy currents on the plant's dynamics will appear primarily at higher frequencies. Furthermore, the effect will be apparent at all values of nominal gap.

VI. NONLAMINATED ACTUATOR EXPERIMENT

A. Setup

A labeled photograph of the experimental system is presented in Fig. 7. A stainless steel beam (175 mm × 37.5 mm × 25 mm, 1.49 kg), supported by a compliant aluminum flexure (3.23 N/mm), is constrained to 1-DOF translation. A nonlaminated magnetic actuator and an electrodynamic shaker are located on opposite ends of the beam. The motion of the beam can be measured with both a noncontact Bentley 7200 displacement sensor and a PCB Model 352C65 ICP accelerometer.

The flotor of the nonlaminated magnetic actuator is attached to the beam and the stator is attached to an actuator stand, which is bolted to a steel base plate. The flotor and the stator are machined from solid pieces of Carpenter's Hyperm 49 magnetic alloy (dry hydrogen annealed). To investigate the magnetic

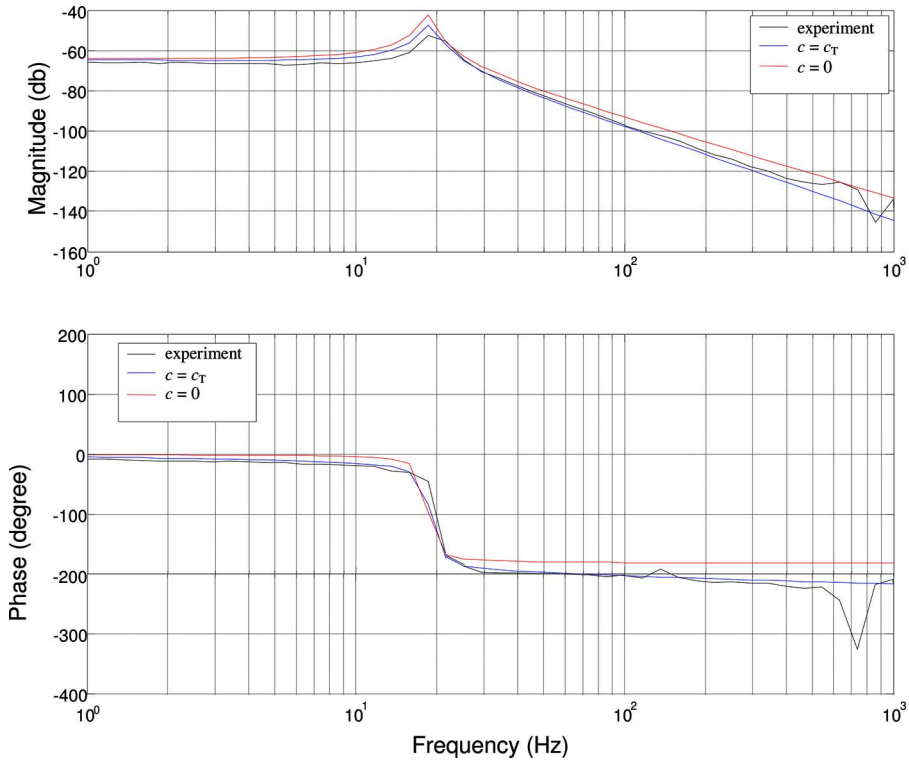

Fig. 8. Frequency response of nonlaminated experiment, $X(s)/I_p(s)$, and model, with and without eddy current effects.

properties of this material, a Rowland ring test was conducted on a test sample. This test indicated a relative permeability of 9000 and a coercive force of 0.1 Oe. The flotor and stator dimensions and properties are summarized in Table II. The nonlaminated actuator was powered by a Krohn-Hite 7500 linear power amplifier and the actuator coil current was measured by a calibrated LEM HY10-P current transducer. Since the current-mode and voltage-mode models differ only in whether Faraday's law (45) is included in the model description, only current-mode experimental results are presented.

The shaker employed is a *Labworks* ET-132-2, a linear Lorentz actuator, powered by *Labworks* PA-138-1 linear amplifier. The shaker is attached to the beam and is bolted to the shaker base. Both the base plate and shaker base are attached to a milling machine bed for a foundation. Frequency responses were measured via a HP 3566A PC spectrum/network analyzer.

B. Modeling

The mechanical subsystem of the experiment (beam, flotor, and flexures) may be modeled with the transfer function

$$H(s) = \frac{1}{ms^2 + c_m s + K_m} \tag{52}$$

where m is the effective mass, and c_m and K_m are the damping and stiffness coefficients provided to the mechanical system by the flexure and shaker armature. With this model, the transfer function between current and displacement, (43), may be simplified as (53), shown at the bottom of the page

Calibration tests were conducted to determine all the parameters with the exception of that associated with eddy current effect c.

Flexure stiffness was determined by applying known forces to the beam via the calibrated shaker and measuring the resulting displacement using the position sensor ($K_m = 34924\,\mathrm{N/m}$). The damping of the mechanical subsystem was determined by sine-sweep testing with the shaker as the excitation source and subsequent parameter identification ($c_m = 20.014$ N·s/m). The effective mass of the mechanical subsystem was 2.205 kg.

The actuator parameter K_x was found via the following process: 1) set the nominal current i_0 and gap g_0, and record the initial position of the beam; 2) using the shaker, apply forces so as to pull the flotor away from the nonlaminated stator and increase the air gap length approximately 1.25 μm (0.005 in); 3) decrease the current applied to the shaker in a series of small steps until the air gap length is approximately 1.25 μm smaller than the nominal value g_0, and record the shaker current and beam position at each step. The data obtained by this process indicate the relationship between the attractive force generated by the nonlaminated actuator and the air gap length, as described by (1). These data are curve-fitted with the function $f = \upsilon_g / g^2$ to determine parameter υ_g. Evaluating $df/dg|_{g=g_0}$

$$\frac{X(s)}{I_p(s)} = \frac{K_i R^0}{\left\{cms^{5/2} + R^0 ms^2 + cc_m s^{3/2} + R^0 c_m s + cK_m s^{1/2} + R^0 (K_m - K_x)\right\}} \tag{53}$$

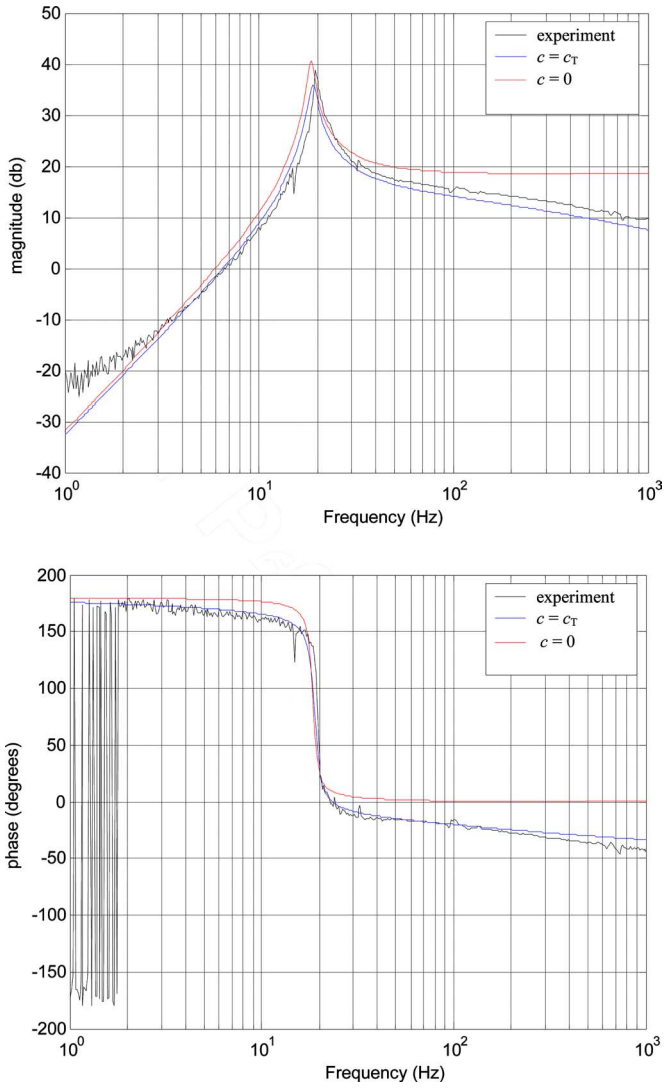

Fig. 9. Frequency response of experiment, $A(s)/I_p(s)$, and theoretical model, with and without eddy currents.

then yields K_x. With $g_0 = 510.5$ μm (0.0201 in) and $i_0 = 0.15$ A, the calibration test yields $K_x = 5478\,\mathrm{N/m}$. Using a flux leakage factor of 0.60 obtained from finite-element analysis, a theoretical value of K_x was calculated to be $K_x = 5339\,\mathrm{N/m}$, which is quite close to the experimental value.

The actuator current gain K_i was found by the following process: 1) set the nominal gap g_0 and record the initial position of the beam; 2) apply a constant current to the nonlaminated actuator so as to cause a displacement of the beam; and 3) increase the shaker armature current until the beam is brought back to its original position, and record the shaker and nonlaminated actuator currents. Using a range of values for the nonlaminated actuator current in this procedure will specify the relationship between attractive force generated by and current applied to the nonlaminated actuator, as described by (1). Fitting the data with a function of the form $f = v_i\, i^2$ and evaluating $df/di|_{i=i_0}$ yields the actuator gain K_i. With $g_0 = 510.5$ μm and $i_0 = 0.15$ A, the calibration test yields $K_i = 18.67\,\mathrm{N/A}$. The theoretical value of K_i calculated with a flux leakage factor of 0.60 is $K_i = 18.38\,\mathrm{A/m}$.

Substitution of the nonlaminated actuator's material and geometric properties into (39b) and Table I yields a theoretical value (subscript *T*) for the eddy current coefficient: $c_T = 14710$ A/Wb.

C. Experimental Results

Fig. 8 presents a comparison of experimental data obtained by sine-sweep testing using the nonlaminated actuator and the calculated frequency responses of plant transfer function $X(s)/I_p(s)$ (53) using $c = c_T$ and $c = 0$ (no eddy currents). (The shaker was connected during the test as it is part of the identified mechanical subsystem; it was not activated, however.) The results demonstrate that the analytic model presented accurately predicts the effects of eddy currents upon the dynamics of nonlaminated magnetic actuators. For better comparison at high frequencies, the frequency response was also determined via sine-sweep with the beam accelerometer employed as the output transducer. The theoretical model for this input–output pair is (54), shown at the bottom of the page, where *A*(*s*) is the Laplace transform of the acceleration signal. The experimental data are shown in Fig. 9 along with theoretical curves obtained using $c = c_T$ and $c = 0$. The theoretical prediction closely follows the experimental data. Note that the magnitude at high frequency is attenuating at a rate of 10 dB per decade and the phase is asymptotically approaching -45°. These results are strongly indicative of the fractional order of the system. Both phenomena are predicted by the model (54) whose relative degree is $1/2$.

VII. Conclusion

Two outstanding issues regarding modeling of these nonlaminated magnetic actuators were resolved in this study. First, the effect that continuously varying flotor motion has upon the force applied to the flotor was derived from first principles. Second, the relationship between electromagnet coil voltage and the force induced upon the flotor was resolved. Several key insights were provided regarding the range of air gaps and excitation frequencies that would show the most significant effects of eddy currents. The dynamical model presented is an explicit function of the material and geometric properties of the nonlaminated actuator. As a result, the model is suitable for optimization and tradeoff studies. Experimental results were provided that show close agreement with the theory presented.

$$\frac{A(s)}{I_p(s)} = \frac{K_i R^0 s^2}{\left\{cms^{5/2} + R^0 ms^2 + cc_m s^{3/2} + R^0 c_m s + cK_m s^{1/2} + R^0 (K_m - K_x)\right\}} \tag{54}$$

ACKNOWLEDGMENT

The authors thank Prof. E. Maslen for many helpful discussions. The authors offer their appreciation to Dr. D. Meeker for helpful insights and the use of finite-element analysis code, finite-element method magnetics (FEMM).

REFERENCES

[1] R. Fittro and C. Knospe, "Rotor compliance minimization via mu-control of active magnetic bearings," *IEEE Trans. Control Syst. Technol.*, vol. 10, no. 2, pp. 238–249, Mar. 2002.

[2] M. D. Noh, S.-R. Cho, J.-H. Kyung, S.-K. Ro, and J.-K. Park, "Design and implementation of a fault-tolerant magnetic bearing system for turbomolecular vacuum pump," *IEEE/ASME Trans. Mechatronics*, vol. 10, no. 6, pp. 626–631, Dec. 2005.

[3] H. Hayashiya, D. Iizuka, H. Ohsaki, and E. Masada, "A novel combined lift and propulsion system for a steel plate conveyance by electromagnets," *IEEE Trans. Magn.*, vol. 34, no. 4, pp. 2093–2095, Jul. 1998.

[4] D. L. Trumper, M. Weng, and R. Ritter, "Magnetic suspension and vibration control of beams for non-contact processing," in *Proc. 1999 IEEE Conf. Control Appl.*, Kona, HI, vol. 1, Aug., pp. 551–557.

[5] P. Subrahmanyan and D. Trumper, "Active vibration isolation design for a photolithographic stepper," presented at the 6th Int. Symp. Magn. Bearings, Cambridge, MA, Aug. 1998.

[6] H. Gutierrez and P. Ro, "Sliding-mode control of a nonlinear-input system: Application to a magnetically levitated fast-tool servo," *IEEE Trans. Ind. Electron.*, vol. 45, no. 6, pp. 921–927, Dec. 1998.

[7] R. B. Zmood, D. K. Anand, and J. A. Kirk, "The influence of eddy currents on magnetic actuator performance," *Proc. IEEE*, vol. 75, no. 2, pp. 259–260, Feb. 1987.

[8] R. L. Stoll, *The Analysis of Eddy Currents*. London, U.K.: Oxford Univ. Press, 1974.

[9] J. J. Feeley, "A simple dynamic model for eddy currents in a magnetic actuators," *IEEE Trans. Magn.*, vol. 32, no. 2, pp. 453–458, Mar. 1996.

[10] L. Zhu, C. Knospe, and E. Maslen, "An analytical model of a nonlaminated cylindrical magnetic actuator including eddy currents," *IEEE Trans. Magn.*, vol. 41, no. 4, pp. 1248–1258, Apr. 2005.

[11] L. Kucera and M. Ahrens, "A model for axial magnetic bearings including eddy currents," in *Proc. 3rd Int. Symp. Magn. Suspension Technol.*, Tallahassee, FL, Dec.1995, pp. 421–436.

[12] L. Zhu, C. Knospe, and E. Maslen, "Frequency domain modeling of nonlaminated C-shaped magnetic actuators," in *Proc. 9th Int. Symp. Magn. Bearings*, Lexington, KY, Aug. 2004, pp. 1–6.

[13] C. Bonnet and J. R. Partington, "Coprime factorizations and stability of fractional differential systems," *Syst. Control Lett.*, vol. 41, no. 3, pp. 167–174, Oct. 2000.

Lei Zhu received the B.S. degree in electrical engineering from Hefei University of Technology, Hefei, China, in 1995, the M.S. degree in control engineering from the University of Science and Technology of China, Hefei, in 1998, and the Ph.D. degree in mechanical and aerospace engineering from the University of Virginia, Charlottesville, in 2005.

He is currently with Calnetix, Inc., Cerritos, CA, where he is engaged in the development high-speed rotating machinery supported by magnetic bearings. His current research interests include electromechanical system design, analysis, and control.

Carl R. Knospe (S'88–M'88–SM'07) received the B.S. degree in aerospace engineering and the Ph.D. degree in mechanical and aerospace engineering from the University of Virginia, Charlottesville, in 1984 and 1989, respectively.

In 1989, he joined the University of Virginia, where he is currently an Associate Professor in the Department of Mechanical and Aerospace Engineering. His work has considered the active control of vibration, the design of high-performance actuators, active magnetic suspension, the control of machining chatter, and the analysis of time-delay systems. He is the author or coauthor of more than 40 journal publications.

Prof. Knospe is currently an Associate Editor for the IEEE TRANSACTIONS ON CONTROL SYSTEMS TECHNOLOGY and the IEEE Control Systems Magazine. He received Best Paper awards at both the 5th and 6th International Symposia on Magnetic Bearings (Kanazawa, Japan; Cambridge, MA).